

## Strain relaxation properties of $\text{InAs}_y\text{P}_{1-y}$ metamorphic materials grown on InP substrates

Mantu K. Hudait,<sup>a)</sup> Y. Lin, and S. A. Ringel<sup>b)</sup>

*Department of Electrical and Computer Engineering, The Ohio State University, Columbus, Ohio 43210, USA*

(Received 31 October 2008; accepted 10 February 2009; published online 25 March 2009)

The strain relaxation mechanism and defect properties of compositionally step-graded  $\text{InAs}_y\text{P}_{1-y}$  buffers grown by molecular beam epitaxy on InP have been investigated. InAsP layers having lattice misfits ranging from 1% to 1.4% with respect to InP, as well as subsequently grown lattice matched  $\text{In}_{0.69}\text{Ga}_{0.31}\text{As}$  overlayers on the metamorphic buffers were explored on both (100) and  $2^\circ$  offcut (100) InP substrates. The metamorphic graded buffers revealed very efficient relaxation coupled with low threading dislocation densities on the order of  $(1-2) \times 10^6 \text{ cm}^{-2}$  for the range of misfit values explored here. A detailed analysis via high resolution x-ray diffraction revealed that the strain relaxed symmetrically, with equivalent numbers of  $\alpha$  and  $\beta$  dislocations, and to greater than 90% for all cases, regardless of substrate offcut. Further analysis showed the relaxation to always be glide limited in these materials when grown on a graded buffer compared to a single step layer. The threading dislocation density was observed by plan-view transmission electron microscopy to be constant for the range of misfit values studied here in the top layer of the graded structures, which is attributed to the very efficient use of residual dislocations and the dominance of dislocation glide over nucleation in these graded anion metamorphic buffers, suggesting great promise for metamorphic devices with lattice constants greater than that of InP to be enabled by InAsP metamorphic structures on InP. © 2009 American Institute of Physics. [DOI: [10.1063/1.3098232](https://doi.org/10.1063/1.3098232)]

### I. INTRODUCTION

Compositionally step-graded  $\text{InAs}_y\text{P}_{1-y}$  alloys are of a great promise to create “virtual” substrates between the InP and InAs semiconductors. These metamorphic buffers generate an engineered substrate platform for device structures to access the rich band structure available in the lattice constants out to InAs but would be based on InP wafer technology. To date, several types of devices have been developed on high-quality metamorphic InAsP buffers,<sup>1-10</sup> whose lattice constants are controlled via grading of the group-V anion sublattice, as opposed to the more usual group-III cation sublattice,<sup>11-21</sup> as this approach enables separation of control of growth rate from strain introduction rate, especially for the molecular beam epitaxial (MBE) growth technique.<sup>1,22</sup> Low band gap,  $\text{In}_x\text{Ga}_{1-x}\text{As}$ -based thermophotovoltaic (TPV) devices, which receive substantial interest for energy conversion applications, also exploit metamorphic buffers to reach their band gap range of interest, 0.5–0.6 eV for InGaAs devices on InP. To date, several groups have successfully applied  $\text{InAs}_y\text{P}_{1-y}$  metamorphic buffers on InP substrates for high-performance lattice mismatched  $\text{In}_x\text{Ga}_{1-x}\text{As}$  TPV devices,<sup>1-6</sup> and the outstanding device performance is largely due to the success of the low arsenic-composition ( $< \sim 40\%$ ) part of the  $\text{InAs}_y\text{P}_{1-y}$  alloy system used in this application. Recently, we have demonstrated high electronic quality and very high bulk mobilities of relaxed, high arsenic

content InAsP layers up to pure InAs grown by MBE using step-graded  $\text{InAs}_y\text{P}_{1-y}$  buffers on InP substrates through detailed transport studies, indicating that high-quality mismatched devices can be achieved on these  $\text{InAs}_y\text{P}_{1-y}$  graded buffers from InP to InAs.<sup>23-25</sup> With such demonstrations as motivation, it is necessary to determine how to fully optimize the promising metamorphic InAsP buffer, and this requires study of strain relaxation mechanisms.

Mixed-anion III-V semiconductor alloys have advantages over mixed-cation III-V alloys in compositionally graded, lattice mismatched epitaxy. Since two group-III elements having unity sticking coefficients but with different surface mobilities take part in the growth of mixed-cation materials, the change in the difference of their respective adatom surface mobilities from one composition to the next may cause randomized nucleation during the growth and may thus lead to the formation of alloy decomposition/branch defects, which generates severe surface roughness and blocking of dislocation glide during strain relaxation.<sup>26-28</sup> In contrast, mixed-anion semiconductors do not have this issue in the growth because only one group-III element is involved. Furthermore, in the growth of mixed-anion semiconductors, the group-III flux determines the growth rate and the two group-V species control the chemical composition; hence the lattice constant and the growth rate are decoupled, which offers a potential advantage for the growth of mixed-anion semiconductor alloys. With regard to mixed-anion-graded buffers, this advantage also provides more degrees of freedom in the optimization of the strain relaxation in these structures. However, compared with mixed-cation III-V metamorphic epitaxy,<sup>29-32</sup> information re-

<sup>a)</sup>Present address: Components Research, Intel Corporation, Hillsboro, OR 97124. Electronic mail: mantu.k.hudait@intel.com.

<sup>b)</sup>Author to whom correspondence should be addressed. Tel.: (614) 292-6904; FAX: (614) 292-9562; Electronic mail: ringel.5@osu.edu.

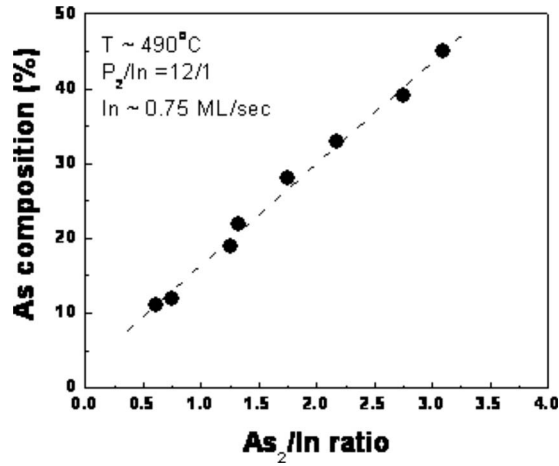


FIG. 1. As content as a function of  $\text{As}_2/\text{In}$  flux ratios in  $\text{InAs}_y\text{P}_{1-y}$  layers as determined by triple axis XRD.

guarding the nature of strain relaxation in mixed-anion-graded buffers is relatively sparse and focused on material grown by metal-organic chemical vapor deposition.<sup>33,34</sup> This is due largely to the traditional ease with which compositions (and therefore equilibrium lattice constants) can be controlled in the mixed-cation systems due to the unity sticking coefficients of the group-III species at growth temperature. In fact, several groups succeeded in growing highly relaxed mixed-cation-graded buffer layers with nearly ideal strain relaxation properties. This paper presents a comprehensive study of strain relaxation properties in mixed-anion, step-graded  $\text{InAs}_y\text{P}_{1-y}$  buffers grown by solid source MBE. The results complement and extend earlier studies on both single step lattice mismatched  $\text{InAsP}$  layers on  $\text{InP}$  (Refs. 35–38) and on the much more extensively studied cation-graded III-V metamorphic materials.<sup>11–21</sup> Here, comparative studies are made on both (100) and  $2^\circ$  offcut (100)  $\text{InP}$  substrates with arsenic composition ranges from  $y=0.28$ – $0.45$ , which represents a range of total misfit from 1.0% to 1.4% with respect to the  $\text{InP}$  substrate. In order to better elucidate the kinetic process of strain relaxation within the  $\text{InAs}_y\text{P}_{1-y}$  graded buffer layers, comparisons are also made with lattice matched  $\text{In}_{0.69}\text{Ga}_{0.31}\text{As}$  overlayers grown on the virtual  $\text{InAs}_y\text{P}_{1-y}/\text{InP}$  substrates and with single step, relaxed  $\text{InAs}_y\text{P}_{1-y}$  layers grown on  $\text{InP}$ .

## II. EXPERIMENTAL

### A. Growth of $\text{InAs}_y\text{P}_{1-y}$ step-graded buffer layers

Single composition and compositionally step-graded  $\text{InAs}_y\text{P}_{1-y}$  layers ( $y=0.10$ – $0.45$ ) were grown by solid source MBE on both (100) and offcut (100)  $\text{InP}$  substrates ( $2^\circ$  off toward the  $[110]$  direction) after the growth of  $0.2 \mu\text{m}$  undoped  $\text{InP}$  buffer under a stabilized phosphorus flux with an average grading rate of  $20\% \text{As}/\mu\text{m}$ . In all cases, a strong ( $2 \times 4$ ) reflection high-energy electron diffraction (RHEED) pattern was consistently observed throughout the  $\text{InAs}_y\text{P}_{1-y}$  growth. The growth rate for all  $\text{InAs}_y\text{P}_{1-y}$  layers was maintained at  $\sim 0.75 \text{ML/s}$ , as determined by RHEED intensity oscillations and a constant growth temperature of  $\sim 490^\circ\text{C}$  was used, as measured by an optical pyrometer. Figure 1

shows the measured arsenic content as a function of the  $\text{As}_2/\text{In}$  MBE beam flux ratio for  $\text{InAsP}$  test layers used to calibrate growths for this study. All compositional data were obtained from triple axis x-ray diffraction (XRD) measurements. For the graded structures, the first three undoped step-graded layers were each grown to a thickness of  $0.4 \mu\text{m}$ , followed by a final  $1.5 \mu\text{m}$  thick  $\text{InAs}_y\text{P}_{1-y}$  ( $y=0.28$ – $0.45$ ) layer on both types of  $\text{InP}$  substrates. The range of compositions for the thick  $\text{InAsP}$  cap layers translates to a total misfit of  $\sim 1.0\%$ – $1.4\%$  with respect to the original  $\text{InP}$  substrate. Full growth details can be found in earlier publications.<sup>1,22</sup>

### B. Structural characterization and strain relaxation calculations for $\text{InAsP}$ buffers

The strain relaxation and defect properties of the step-graded buffers were characterized using triple axis XRD, cross-sectional transmission electron microscopy (XTEM), and plan-view TEM. TEM samples were prepared using both focused ion beam (FIB) processing and conventional chemical-mechanical thinning procedure followed by Ar ion milling. Triple axis XRD measurements were carried out with a Bede Scientific Instruments D1 system using the  $\text{Cu } K\alpha_1$  line. Two sets of reciprocal space maps (RSMs), the symmetric (004) and asymmetric (115), were measured in order to determine the alloy composition, the lattice mismatch, and the strain relaxation in each  $\langle 110 \rangle$  in-plane direction. Since misfit dislocations relieve epilayer strain, an asymmetry in misfit dislocation (MD) density should result in different in-plane lattice constants in the two orthogonal  $[110]$  and  $[1\bar{1}0]$  dislocation directions. With these data, the epilayer in-plane and out-of-plane lattice constants can be determined along the two orthogonal  $\langle 110 \rangle$  directions. The relaxed lattice constant  $a_r$  and the state of strain  $\varepsilon$  for the  $[110]$  direction can be determined for cubic heteroepitaxial layers using<sup>1,39</sup>

$$a_{r[110]} = \frac{1-\nu}{1+\nu} a_{\perp[110]} + \frac{\nu}{1+\nu} a_{\parallel[110]}, \quad (1)$$

$$\varepsilon_{\text{in-plane}} = \frac{a_{\parallel[110]} - a_{r[110]}}{a_{r[110]}}, \quad (2)$$

and

$$\varepsilon_{\text{out-of-plane}} = \frac{a_{\perp[110]} - a_{r[110]}}{a_{r[110]}}, \quad (3)$$

where  $\nu$  is Poisson's ratio of each ternary layer calculated from the elastic constants of  $\text{InAs}$  and  $\text{InP}$  using Vegard's law,<sup>39</sup>  $a_{\perp[110]}$  and  $a_{\parallel[110]}$  are the out-of-plane and in-plane lattice constants measured with the projection of the incident beam oriented along the  $[110]$  direction. Similarly, the relaxed layer lattice constant and the in-plane and out-of-plane lattice constants were determined using the above method along the  $[1\bar{1}0]$  direction. From these terms, the relaxation in each  $\langle 110 \rangle$  direction can be expressed as<sup>1,39</sup>

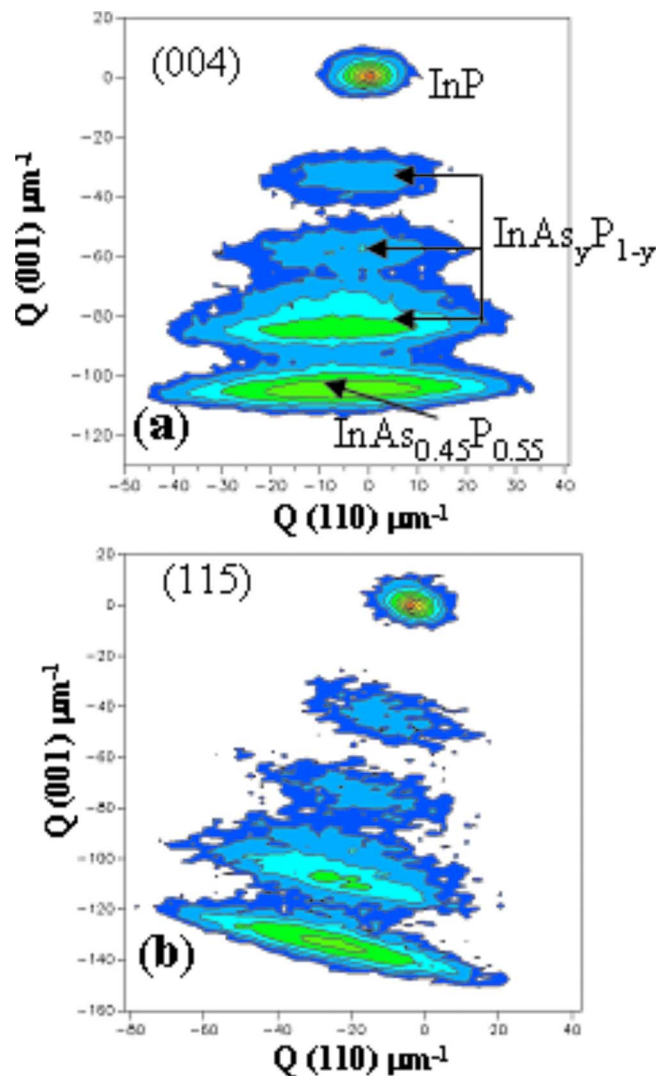


FIG. 2. (Color online) (a) Symmetric (004) and (b) asymmetric (115) RSMs of an  $\text{InAs}_{0.45}\text{P}_{0.55}/\text{InAs}_y\text{P}_{1-y}$  step-graded buffer grown on a (001) InP substrate obtained using an incident beam along the  $[110]$  direction.

$$R_{[110]} = \frac{a_{\parallel[110]} - a_o}{a_{r[110]} - a_o} \quad \text{and} \quad R_{[1\bar{1}0]} = \frac{a_{\parallel[1\bar{1}0]} - a_o}{a_{r[1\bar{1}0]} - a_o}, \quad (4)$$

where  $a_o$  is the equilibrium lattice parameter of the InP substrate.

### III. RESULTS AND DISCUSSION

#### A. Strain relaxation properties

##### 1. $\text{InAs}_y\text{P}_{1-y}$ step-graded buffer on on-axis and offcut (100) InP substrates

The relaxation state and the residual strain of each buffer layer were obtained from symmetric (004) and asymmetric (115) reflections of RSMs measured using triple axis XRD. Figures 2 and 3 show the RSMs for (004) and (115) reflections obtained from a  $1.5 \mu\text{m}$  thick  $\text{InAs}_{0.45}\text{P}_{0.55}$  epitaxial layer grown on an on-axis (001) InP substrate using a three step  $\text{InAs}_y\text{P}_{1-y}$  graded buffer layer, with the incident beam along the  $[110]$  and  $[1\bar{1}0]$  directions, respectively. The (004) RSMs exhibit five distinct reciprocal lattice point (RLP) maxima, and the peak assignments corresponding to those

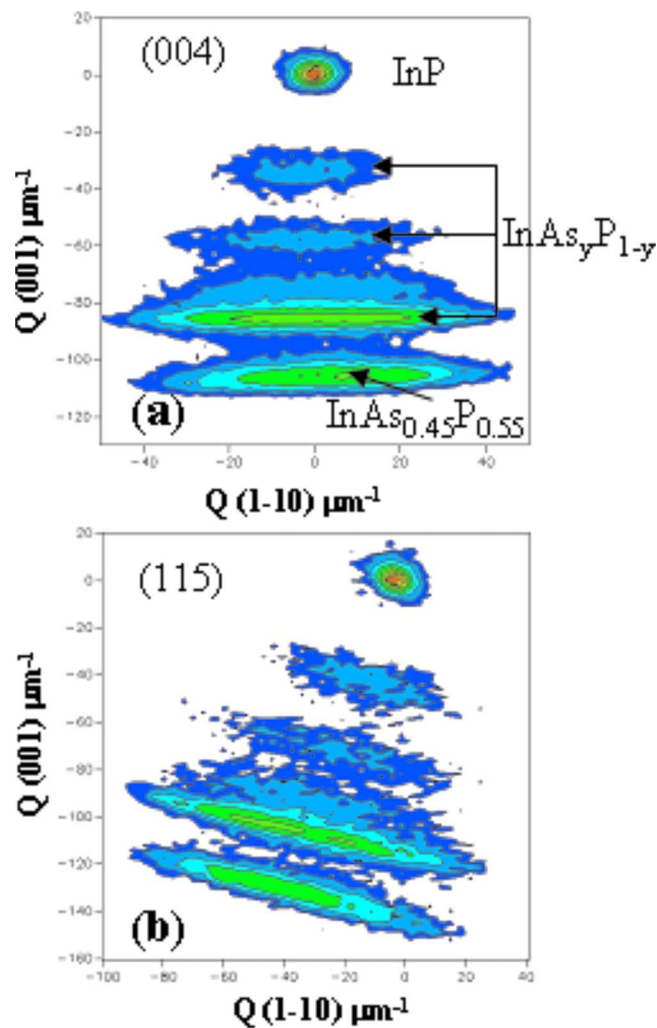


FIG. 3. (Color online) (a) Symmetric (004) and (b) asymmetric (115) RSMs of an  $\text{InAs}_{0.45}\text{P}_{0.55}/\text{InAs}_y\text{P}_{1-y}$  step-graded buffer grown on a (001) InP substrate obtained using an incident beam along the  $[1\bar{1}0]$  direction.

RLP maxima are from (i) the InP substrate, (ii) the first InAsP buffer, (iii) the second InAsP buffer, (iv) the third InAsP buffer, and (v) the final  $\text{InAs}_{0.45}\text{P}_{0.55}$  layer. From these RSMs, one can determine the lattice parameter in the growth plane,  $a_{\parallel}$  (from the asymmetric reflection), and the lattice parameter in the out-of-plane (growth direction),  $a_{\perp}$  (from the symmetric reflection), in the two orthogonal  $\langle 110 \rangle$  directions. The degree of relaxation of the overlayer can be calculated from the measured lattice parameters and the Poisson's ratio with respect to the InP substrate. Using RSMs from Fig. 2, the measured lattice constants along the out-of-plane and in-plane directions of the top  $\text{InAs}_{0.45}\text{P}_{0.55}$  layer were found to be  $5.9609$  and  $5.9465 \text{ \AA}$ , respectively, with the projection of the beam oriented along the  $[110]$  direction. Similarly, the lattice parameters along the out-of-plane and in-plane directions of the top  $\text{InAs}_{0.45}\text{P}_{0.55}$  layer with the projection of the beam oriented along the  $[1\bar{1}0]$  direction using Figs. 3(a) and 3(b) were found to be  $5.9606$  and  $5.9440 \text{ \AA}$ , respectively. With this information and by using Eqs. (1) and (4), the degree of relaxation of the  $\text{InAs}_{0.45}\text{P}_{0.55}$  layer was calculated to be more than 90%, leaving a residual strain of  $\sim 0.1\%$  in each  $\langle 110 \rangle$  direction, indicating that the relaxation

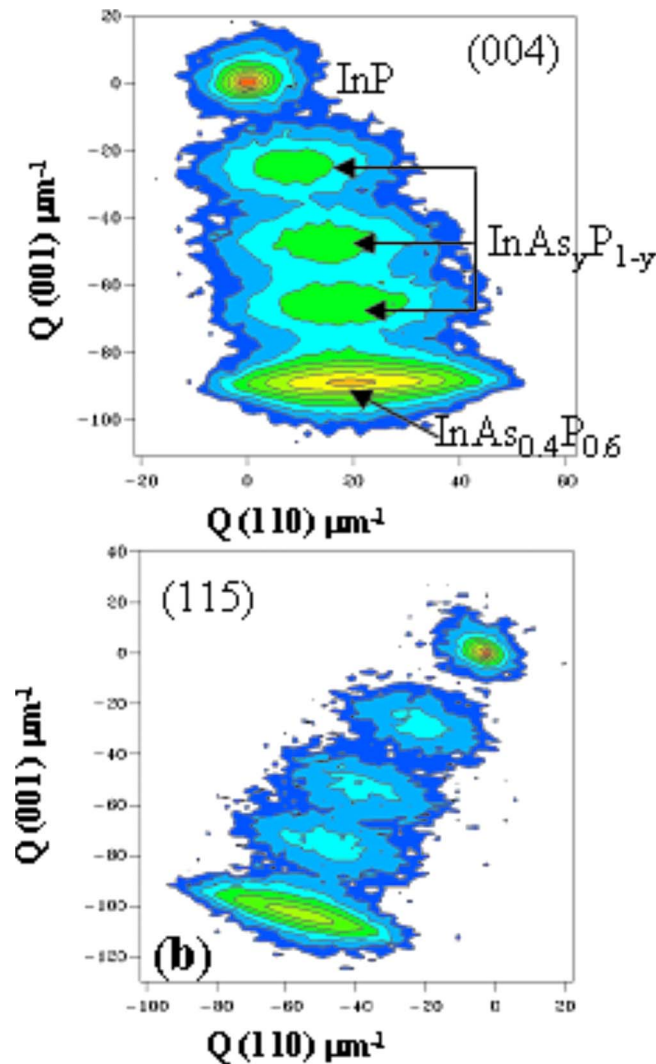


FIG. 4. (Color online) (a) Symmetric (004) and (b) asymmetric (115) RSMs of an  $\text{InAs}_{0.4}\text{P}_{0.6}/\text{InAs}_y\text{P}_{1-y}$  step-graded buffer grown on a  $2^\circ$  offcut (001) InP substrate obtained using an incident beam along the  $[110]$  direction.

is symmetric. One can also find from RSMs in Figs. 2 and 3 that the RLP for each layer in the graded buffer is almost centered on the line extending between the substrate RLP and  $Q=0$  in the two orthogonal  $\langle 110 \rangle$  directions, indicating that each layer in the graded buffer possesses minimum lattice tilt with respect to the substrate.

A similar analysis was performed on a  $1.5 \mu\text{m}$  thick  $\text{InAs}_{0.4}\text{P}_{0.6}$  epitaxial layer grown using a nominally identical  $\text{InAs}_y\text{P}_{1-y}$  graded buffer structure as used above, but now the growth occurs on a (001) InP substrate with a  $2^\circ$  offcut toward the  $[110]$  direction. Figures 4 and 5 show RSMs for (004) and (115) reflections obtained from these offcut samples, with the incident beam along the  $[110]$  and  $[1\bar{1}0]$  directions, respectively. In Figs. 4(a) and 4(b), the measured lattice constants along the out-of-plane and in-plane directions of the top  $\text{InAs}_{0.4}\text{P}_{0.6}$  layer were found to be  $5.9457$  and  $5.9334 \text{ \AA}$ , respectively, with the projection of the beam oriented along the  $[110]$  direction. Similarly, the lattice parameters along the out-of-plane and in-plane directions of the top  $\text{InAs}_{0.4}\text{P}_{0.6}$  layer were found to be  $5.9467$  and  $5.9326 \text{ \AA}$ , respectively, with the projection of the beam oriented along

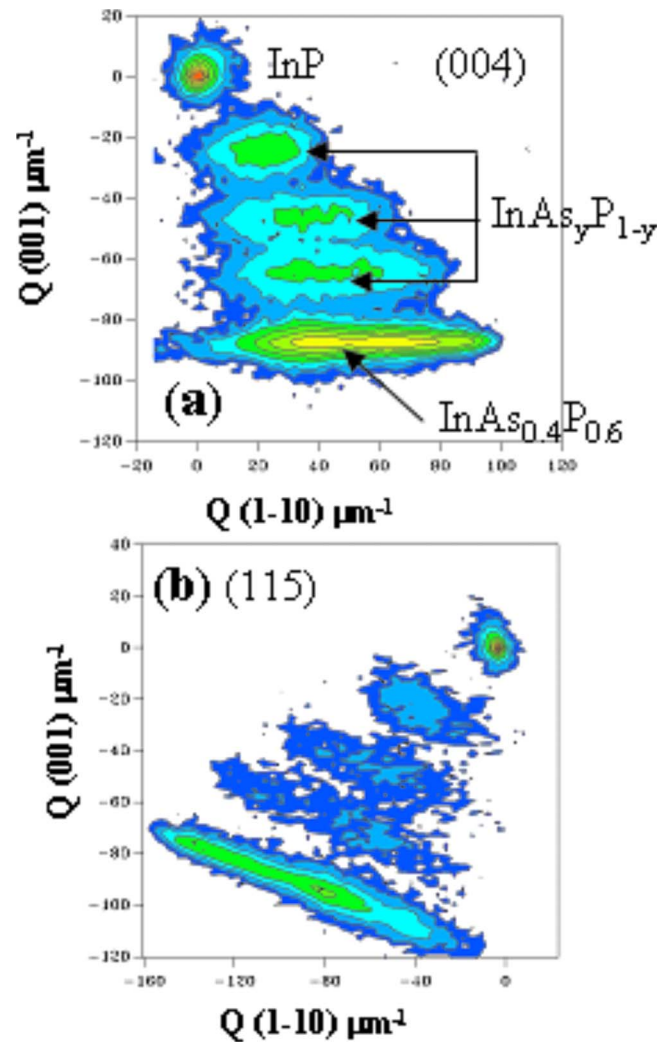


FIG. 5. (Color online) (a) Symmetric (004) and (b) asymmetric (115) RSMs of an  $\text{InAs}_{0.4}\text{P}_{0.6}/\text{InAs}_y\text{P}_{1-y}$  step-graded buffer grown on a  $2^\circ$  offcut (001) InP substrate obtained using an incident beam along the  $[1\bar{1}0]$  direction. A lattice curvature was observed in this direction.

the  $[1\bar{1}0]$  direction using Figs. 5(a) and 5(b). The degree of relaxation of the top  $\text{InAs}_{0.4}\text{P}_{0.6}$  layer were also found to be more than 90% along with the measured values of in-plane and out-of-plane lattice constants in each  $\langle 110 \rangle$  direction, within the relative experimental error, indicating symmetric relaxation.

The values of strain relaxation of the final InAsP layer as a function of arsenic composition for all metamorphic growths with respect to the InP substrate along with the substrate orientation are tabulated in Table I. As can be seen, regardless of the end point composition between  $\text{InAs}_{0.28}\text{P}_{0.72}$  and  $\text{InAs}_{0.45}\text{P}_{0.55}$ , which represents a total misfit that ranges from 1.0% to 1.4% with respect to either on-axis or offcut (001) InP substrate, layer relaxation is both symmetric and greater than 90%. This indicates that the metamorphic layers have reached their equilibrium cubic structure with no measurable tetragonal distortion and that substantial amounts of both  $\alpha$  and  $\beta$  dislocations have been formed during the strain relaxation process. The symmetric relaxation along the two  $\langle 110 \rangle$  directions in the  $\text{InAs}_y\text{P}_{1-y}$  ( $y=0.28-0.45$ ) layer grown on both on-axis and offcut (001)

TABLE I. Summary of the 1.5  $\mu\text{m}$   $\text{InAs}_y\text{P}_{1-y}$  layer ( $y=0.28-0.45$ ) and  $\text{In}_{0.69}\text{Ga}_{0.31}\text{As}$  overlayers grown on InP substrates using an  $\text{InAs}_y\text{P}_{1-y}$  step-graded buffer.

Sample	Substrate offcut	Final $\text{InAs}_y\text{P}_{1-y}$ layer with As composition ( $y$ )	Lattice mismatch with respect to InP (%)	Number of steps between final $\text{InAs}_y\text{P}_{1-y}$ and InP substrate	Thickness of each step within step-graded layers ( $\mu\text{m}$ )	Relaxation of the final layer measured with respect to InP substrate (%) ( $\pm 3\%$ )		Tilt magnitude (arcsec)
						[110]	$[\bar{1}\bar{1}0]$	
A	2° offcut	0.28	$\sim 1.0$	3	0.4/0.4/0.4	92	91	...
B	2° offcut	0.37	$\sim 1.19$	3	0.4/0.4/0.4	90	91	$\sim 196$
C	2° offcut	0.40	$\sim 1.30$	3	0.4/0.4/0.4	93	95	$\sim 217$
D	(100)	0.40	$\sim 1.30$	3	0.4/0.4/0.4	93	92	$\sim 194$
E	(100)	0.45	$\sim 1.40$	3	0.4/0.4/0.4	91	88	$\sim 20$
F	(100)	0.40	$\sim 1.30$	2.7 $\mu\text{m}$ $\text{InAs}_{0.4}\text{P}_{0.6}$ layer directly grown on a (100) InP substrate		94	95	$\sim 18$
G	(100)	$\text{In}_{0.69}\text{Ga}_{0.31}\text{As}$	$\sim 1.1$	4	0.4/0.4/0.4/0.4	90	92	$\sim 46$
H	2° offcut	$\text{In}_{0.69}\text{Ga}_{0.31}\text{As}$	$\sim 1.1$	4	0.4/0.4/0.4/0.4	86	89	$\sim 198$

substrates using  $\text{InAs}_y\text{P}_{1-y}$  step-graded buffers also implies that the total lengths of MD in the two  $\langle 110 \rangle$  directions are similar. In turn this suggests that both  $\alpha$  and  $\beta$  slip systems in the InAsP material have similar activation energies for dislocation nucleation. The lack of impact of substrate offcut on the degree of asymmetric relaxation (or the lack thereof) is quite different from the typical observation for lattice mismatched III-V epitaxy, for which asymmetric strain relaxation due to the use of vicinal substrates is usually observed.<sup>11,16–19,21,40</sup> We can conclude from the symmetric relaxation observed here that almost equal numbers of  $\alpha$  and  $\beta$  dislocations must be formed during the relaxation process of the graded  $\text{InAs}_y\text{P}_{1-y}$  ( $y=0.28-0.45$ ) layer and that the crystal lattice is nearly equivalent to bulk equilibrium lattice spacing with no tetragonal distortion.

## 2. Single step $\text{InAs}_{0.4}\text{P}_{0.6}$ layer on the InP substrate

In order to obtain a better understanding of the relaxation dynamics within the graded buffer layer just described, we have evaluated the strain relaxation of a single step in which the entire misfit strain is applied at a single interface. The reason we are looking at the single step is to see if the symmetric relaxation we are observing for the graded structure is a function of the anion grading or due to the material system itself. A 2.7  $\mu\text{m}$  thick  $\text{InAs}_{0.4}\text{P}_{0.6}$  layer (to match the total thickness of the entire InAsP/graded  $\text{InAs}_y\text{P}_{1-y}$ /InP structure) was grown at  $\sim 490^\circ\text{C}$  on (001) InP at the same growth rate as used for the step-graded buffer. RSMs obtained from this layer are shown in Figs. 6 and 7 for the two  $\langle 110 \rangle$  orthogonal dislocation directions. From the measured values of in-plane and out-of-plane lattice constants determined from RSMs of Figs. 6 and 7, the amount of strain relaxation of the final  $\text{InAs}_{0.4}\text{P}_{0.6}$  layer was found to be greater than 94% in the two  $\langle 110 \rangle$  orthogonal directions. This reveals symmetric relaxation of this layer, and this symmetric relaxation suggests equivalent amounts of  $\alpha$  and  $\beta$  dislocations are formed during the strain relaxation process. Comparison of the (004) symmetric RSMs, shown in Figs. 6, 7, and 2–5, reveals significantly different peak broadening between the single step and graded mismatched layers. In order

to understand the peak broadening along the two orthogonal  $\langle 110 \rangle$  directions, x-ray topography measurements were performed on a bare InP substrate and this  $\text{InAs}_{0.4}\text{P}_{0.6}$ /InP film. Figures 8(a) and 8(b), respectively, show no measurable misfit dislocations observed for the bare InP substrate, as expected, and an array of misfit dislocations along the two orthogonal  $\langle 110 \rangle$  directions for this single step  $\text{InAs}_{0.4}\text{P}_{0.6}$ /InP interface. As seen, the distribution of dislocation along the  $[\bar{1}\bar{1}0]$  direction is different from the  $[110]$  direction that correlates with the x-ray peak broadening observed in Figs. 6 and 7. The additional broadening observed for the single step layer is attributed to higher dislocation densities, as confirmed by TEM analysis discussed in Sec. III C below.

## 3. Properties of lattice matched $\text{In}_{0.69}\text{Ga}_{0.31}\text{As}$ overlayers grown on a virtual $\text{InAs}_y\text{P}_{1-y}$ /InP substrate

In Sec. III A 1, we have demonstrated that  $\text{InAs}_y\text{P}_{1-y}$  graded buffer layer (GBL) relaxes its lattice mismatch strain with underlying InP substrates in a symmetrical fashion. Here we explore if this property is maintained after the growth of InGaAs that is “internally” lattice matched to the cap layer of the InAsP graded buffer, essentially characterizing the metamorphic InAsP buffer as a virtual substrate on InP with an adjustable lattice constant. To carry out this study, 2.5  $\mu\text{m}$  thick  $\text{In}_{0.69}\text{Ga}_{0.31}\text{As}$  overlayers were grown on virtual InAsP substrates using both (001) and 2° offcut (001) InP wafers. Figures 9 and 10 show the RSMs for (004) and (115) reflections obtained for these structures, with the incident beam along the  $[110]$  direction (the measured  $[\bar{1}\bar{1}0]$  RSMs are not shown). In each figure, the (004) RSMs exhibit five distinct RLPs, which corresponds to the InP substrate, three steps in the  $\text{InAs}_y\text{P}_{1-y}$  graded buffer, and the lattice matched  $\text{In}_{0.69}\text{Ga}_{0.31}\text{As}$  layer. Since the  $\text{In}_{0.69}\text{Ga}_{0.31}\text{As}$  layer RLP lies directly on the  $\text{InAs}_{0.32}\text{P}_{0.68}$  buffer, its in-plane lattice constant is coherent with the uppermost buffer layer, indicating that internally lattice matching has been achieved. Further analysis reveals the InGaAs to be symmetrically relaxed to around 90%, consistent with the underlying InAsP virtual substrate layers.

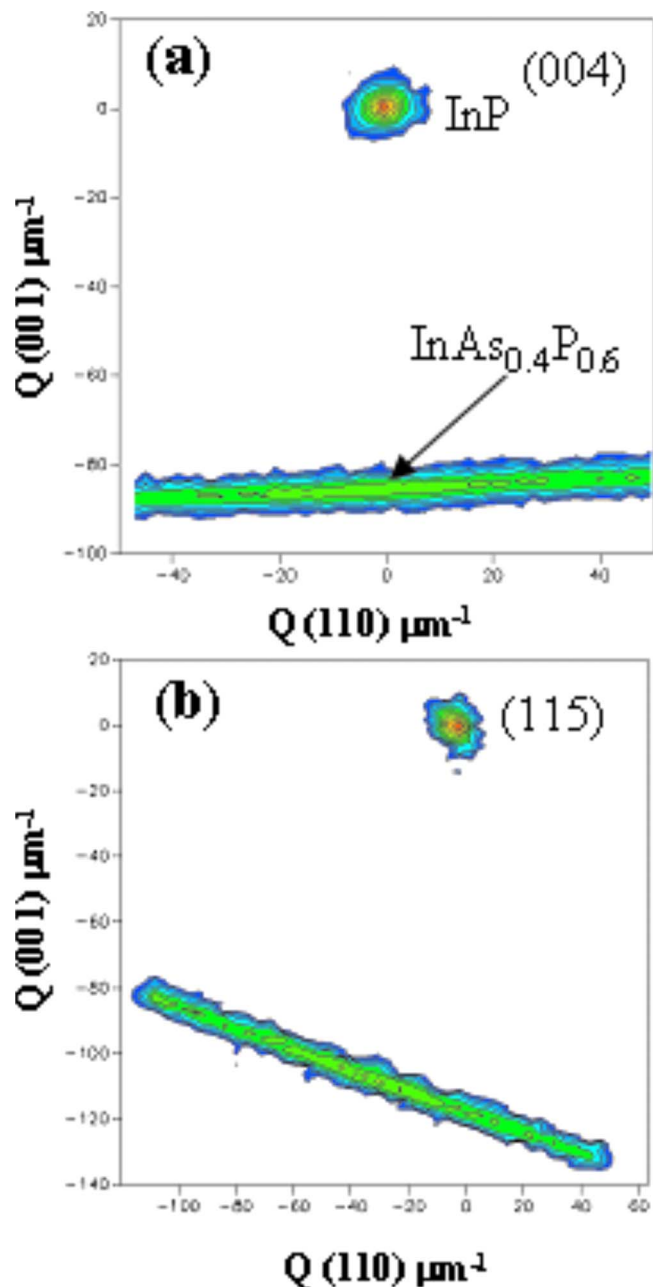


FIG. 6. (Color online) (a) Symmetric (004) and (b) asymmetric (115) RSMs of an  $\text{InAs}_{0.4}\text{P}_{0.6}$  layer directly grown on a (001) InP substrate obtained using an incident beam along the  $[110]$  direction.

## B. Epilayer tilt

Since the tilt of the epitaxial layer is related to the strain relaxation, its measurements could help create a better understanding of the fundamental science of strain relaxation of the graded buffer layers and provide more information about the slip systems that are active during the strain relaxation process. Epilayer tilt is primarily caused by nonzero net out-of-plane Burgers vectors due to the imbalance between dislocation glide/multiplication in different directions. The actual value of tilt with respect to the substrate is found by analyzing the sinusoidal dependence of the XRD peak separation between the substrate and the epilayer as a function of the azimuthal angle of the incoming x-ray beam,<sup>16</sup> with the magnitude of the sine function indicating the degree of tilt.

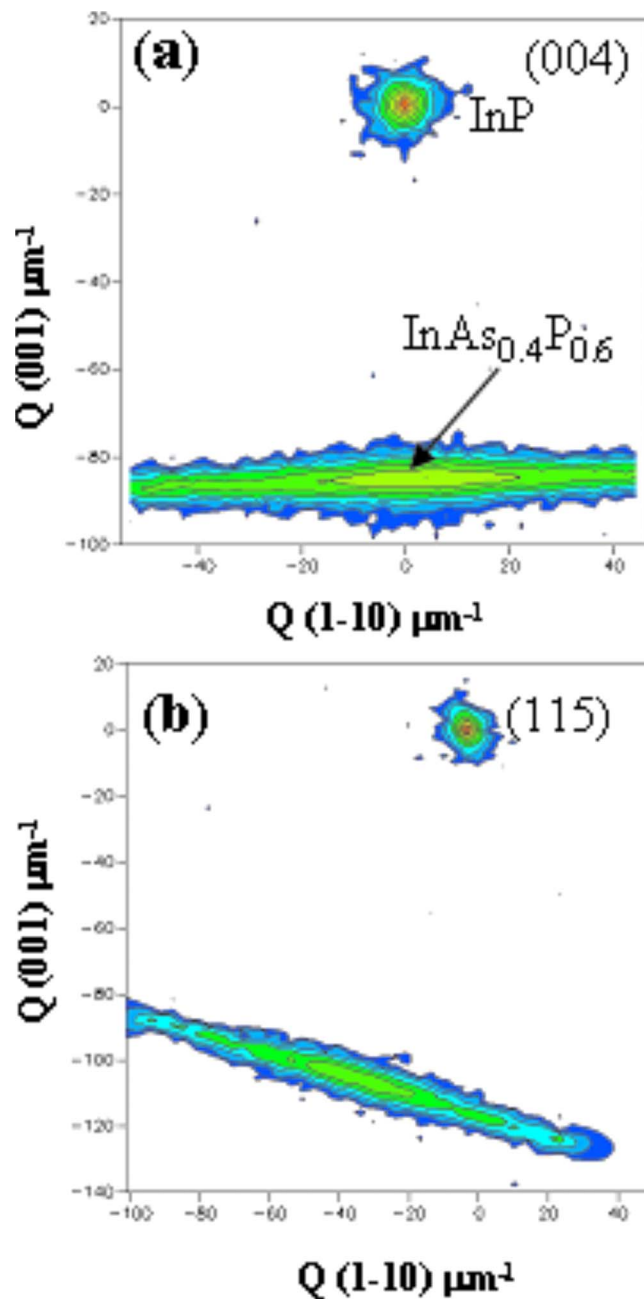


FIG. 7. (Color online) (a) Symmetric (004) and (b) asymmetric (115) RSMs of an  $\text{InAs}_{0.4}\text{P}_{0.6}$  layer directly grown on a (001) InP substrate obtained using an incident beam along the  $[1\bar{1}0]$  direction.

Results are shown in Fig. 11 and Table I, from which we find a negligibly small tilt value of  $\sim 20$  arcsec for the  $\text{InAs}_{0.45}\text{P}_{0.55}$  layer grown using an  $\text{InAs}_y\text{P}_{1-y}$  GBL with respect to the (001) InP substrate. This small lattice tilt amplitude indicates that nearly equal amounts of  $\alpha$  and  $\beta$  dislocations participated during the relaxation process, supporting the conclusion that these layers relax symmetrically from the XRD analysis, above. Small tilt magnitudes ( $\sim 200$  arcsec) were also observed for thick  $\text{InAs}_{0.4}\text{P}_{0.6}$  and  $\text{In}_{0.69}\text{Ga}_{0.31}\text{As}$  cap layers grown on  $\text{InAsP}$  graded buffers on  $2^\circ$  offcut (001) InP substrates. Though a consistently slight increase in tilt angles is observed for the growths on the offcut substrates, the very small magnitude of this tilt implies minimal impact of the substrate offcut on tilt generation at the present growth

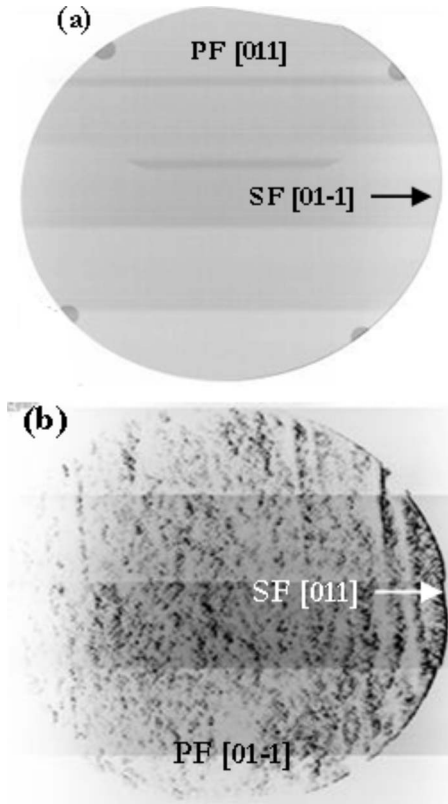


FIG. 8. X-ray topography images of (a) a typical InP substrate and (b) an  $\text{InAs}_{0.4}\text{P}_{0.6}$  layer directly grown on a (001) InP substrate. PF and SF are indicated in this figure as the primary and secondary flats of the wafers.

conditions for the misfit range studied here. A more detailed tilt analysis of Figs. 9 and 10, which lead to Fig. 11 and the listing of data in Table I, shows that the magnitude of lattice tilt present within InGaAs cap layers grown on the graded InAsP buffers matches the value of the final InAsP step in the buffer for both the on-axis and the  $2^\circ$  offcut substrates; i.e., the measured tilt of  $\text{In}_{0.69}\text{Ga}_{0.31}\text{As}$  grown on the offcut substrates is  $\sim 200$  arcsec, similar to the graded InAsP buffer on the offcut substrates, and the measured tilt of  $\text{In}_{0.69}\text{Ga}_{0.31}\text{As}$  grown on the on-axis substrates is  $< 50$  arcsec, matching the range values obtained for the graded InAsP buffer grown on the on-axis substrates. This demonstrates that the strain relaxation of the InGaAs/InAs<sub>y</sub>P<sub>1-y</sub>/InP structures occurs during the growth of the metamorphic InAsP buffer as desired, with negligible lattice tilt, and that the overlying InGaAs layers are internally lattice matched to the final InAsP layer in the graded buffer and thus grow without introduction of additional lattice tilt.

The key point of the above discussion is to show that there is a very small amount of lattice tilt in these samples. Having a negligible epilayer tilt magnitude on the order of  $\sim 200$  arcsec due to substrate offcut suggests that all eight  $60^\circ a/2\langle 110\rangle\{111\}$  slip systems are active in the graded anion buffers. To explain why there is so little tilt, we performed an analysis based on the nucleation-limited tilt model developed by LeGoues *et al.*,<sup>41</sup> where dislocation-dislocation interaction, multiplication, and cross-slip events are not considered. From the magnitude of tilt angle, the fraction of  $60^\circ$

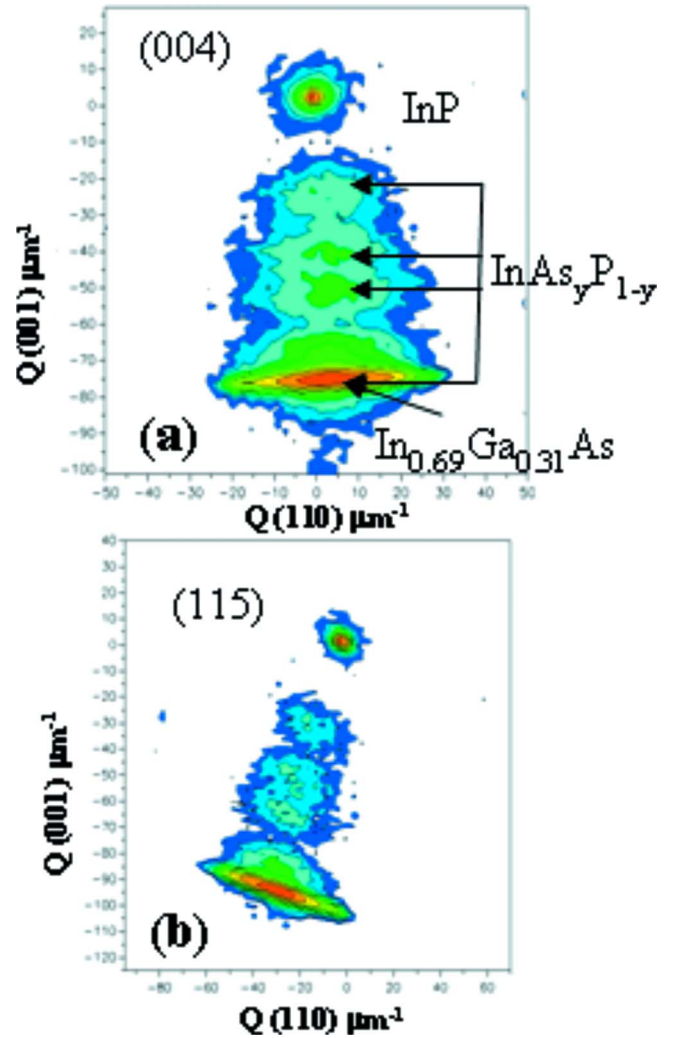


FIG. 9. (Color online) (a) Symmetric (004) and (b) asymmetric (115) RSMs of an  $\text{In}_{0.69}\text{Ga}_{0.31}\text{As}/\text{InAs}_{0.32}\text{P}_{0.68}/\text{InAs}_y\text{P}_{1-y}$  step-graded buffer grown on a (001) InP substrate obtained using an incident beam along the [110] direction.

dislocations with an out-of-plane Burgers vector in a preferred direction responsible for tilt can be calculated using<sup>11</sup>

$$\rho_{\text{tilt}} = \frac{\tan \delta}{|b_{\text{tilt}}|}, \quad (5)$$

where  $\delta$  is the tilt angle,  $\rho_{\text{tilt}}$  is the linear density of misfit dislocation density ( $\text{cm}^{-1}$ ) responsible for the tilt, and  $b_{\text{tilt}}$  is the tilt component of the misfit dislocation, which is in this case  $a_r/2[001]$ . From Eq. (5), for the value of tilt angle of  $\sim 200$  arcsec, the amount of dislocation line density that has a preferred out-of-plane Burgers vector that generates lattice tilt is only  $3.3 \times 10^4 \text{ cm}^{-1}$ , or a net of 6% of Burgers vectors. Thus, the fraction of dislocations responsible for the tilt of the epilayer is very small even on an offcut InP substrate. However, the tilt angle is related to the substrate offcut and the lattice mismatch through the relation,<sup>41</sup>

$$\tan \delta = \varepsilon \frac{b_{\text{tilt}}}{b_{\text{misfit}}} \left( \frac{\exp(-\Delta E_P/kT) - \exp(-\Delta E_N/kT)}{\exp(-\Delta E_P/kT) + \exp(-\Delta E_N/kT)} \right), \quad (6)$$

where  $k$  is the Boltzmann constant,  $b_{\text{misfit}} = a_r/2\sqrt{2}$  is the Burgers vector of misfit dislocation,  $T$  is the growth temperature,

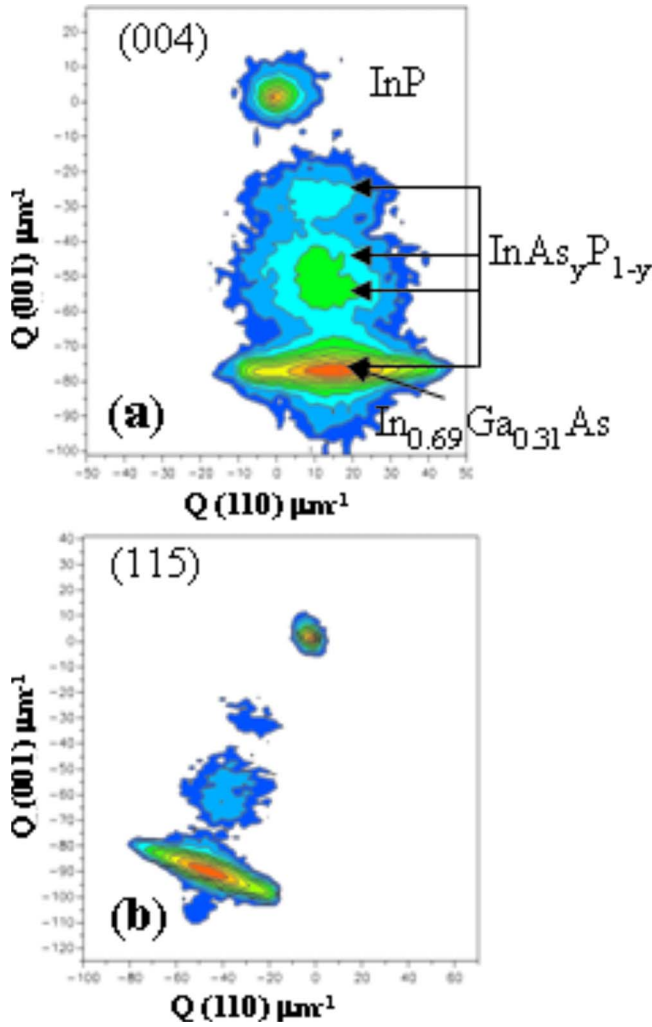


FIG. 10. (Color online) (a) Symmetric (004) and (b) asymmetric (115) RSMs of an  $\text{In}_{0.69}\text{Ga}_{0.31}\text{As}/\text{InAs}_{0.32}\text{P}_{0.68}/\text{InAs}_y\text{P}_{1-y}$  step-graded buffer grown on a  $2^\circ$  offcut (001) InP substrate obtained using an incident beam along the  $[1\bar{1}0]$  direction.

and  $\Delta E_P$  and  $\Delta E_N$  are the change in dislocation nucleation activation energy from  $E_o$  [activation energy for the (001) oriented substrate] for the slip systems generating positive and negative tilt, respectively. Using the small-angle approximation of  $\tan \delta \approx \delta$  and assuming a fully relaxed  $\text{InAs}_{0.4}\text{P}_{0.6}$  layer, the change in nucleation activation energy due to the effect of substrate offcut can be determined. Assuming  $\Delta E_P = -\Delta E_N$  and using the measured lattice tilt of 200 arcsec due to substrate offcut, the change in nucleation activation energy along the  $[110]$  or  $[1\bar{1}0]$  direction is determined to be around 4 meV. This small value for the nucleation activation energy suggests that the strain relaxation of these materials is not due to nucleation-limited and hence negligible lattice tilt.

**C. Dislocation and defects**

Further insight into the structural properties of the various structures analyzed thus far is provided by cross-sectional and plan-view TEM analysis. Figures 12(a) and 12(b) show representative XTEM images of a relaxed  $\text{InAs}_{0.4}\text{P}_{0.6}$  layer grown on a (100) and  $2^\circ$  offcut InP substrate

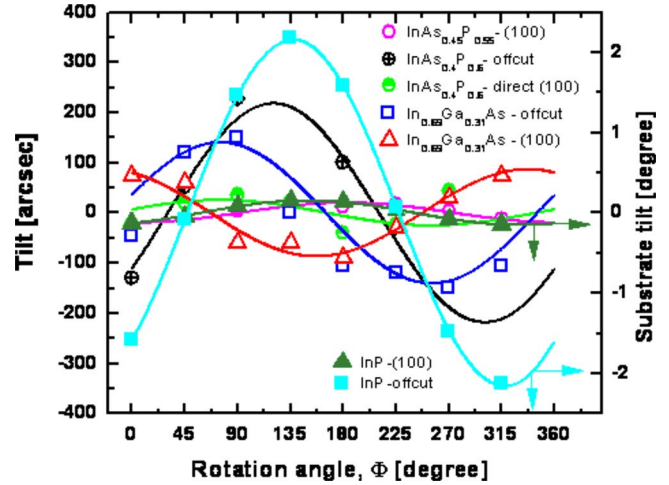


FIG. 11. (Color online) Magnitude of epilayer tilt with respect to the substrate of  $\text{InAs}_{0.4}\text{P}_{0.6}$  and  $\text{In}_{0.69}\text{Ga}_{0.31}\text{As}$  layers grown on (001) and  $2^\circ$  offcut InP substrates using  $\text{InAs}_y\text{P}_{1-y}$  graded buffers along with the substrate tilt.

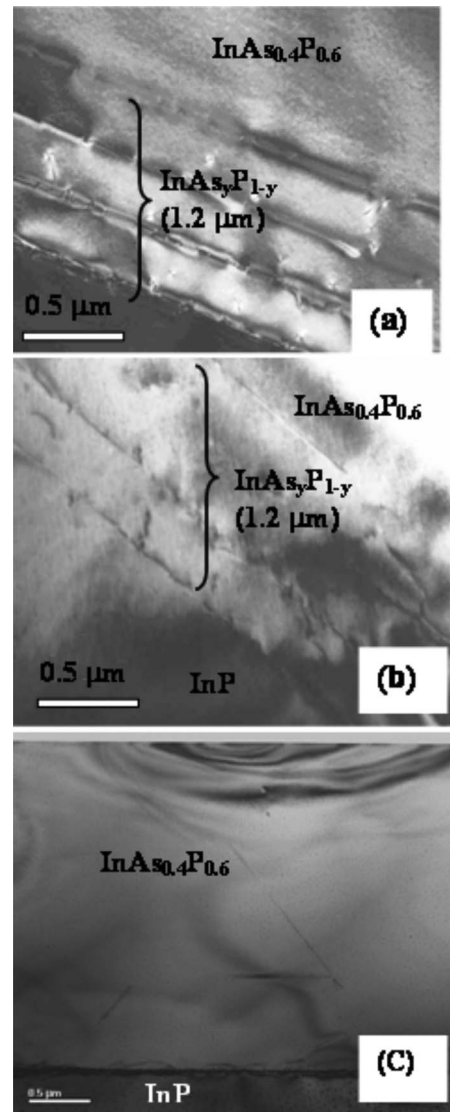


FIG. 12. XTEM images of (a) an  $\text{InAs}_{0.4}\text{P}_{0.6}$  layer grown on a (001) InP (specimen prepared using mechanical polishing and Ar ion milling), (b) an  $\text{InAs}_{0.4}\text{P}_{0.6}$  layer grown on a  $2^\circ$  offcut (001) InP substrate (specimen prepared using FIB) using  $\text{InAs}_y\text{P}_{1-y}$  step-graded buffers, and (c) a direct growth of  $\text{InAs}_{0.4}\text{P}_{0.6}$  on InP. Black dots and black lines are due to indium droplets and bend contour, respectively.

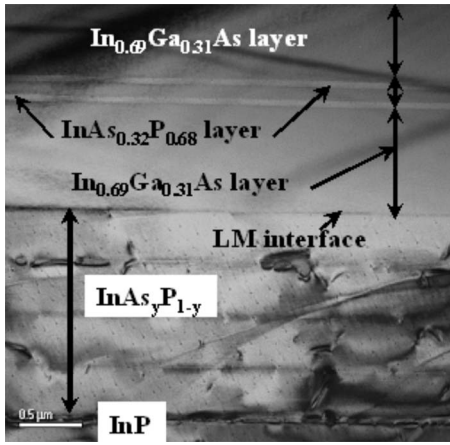


FIG. 13. XTEM image of an  $\text{In}_{0.69}\text{Ga}_{0.31}\text{As}$  overlayer grown on a  $2^\circ$  offcut (001) InP substrate using an  $\text{InAs}_{0.32}\text{P}_{0.68}/\text{InAs}_y\text{P}_{1-y}$  step-graded buffer. An internally lattice matched (LM) composition of an  $\text{InAs}_{0.32}\text{P}_{0.68}$  layer with  $\text{In}_{0.69}\text{Ga}_{0.31}\text{As}$  is shown in this figure. Black dots are due to indium droplets.

using  $\text{InAs}_y\text{P}_{1-y}$  GBL, respectively. These XTEM images show high contrast at the graded buffer layer interfaces due to MDs, with no threading dislocations (TDs) observable in the  $\text{InAs}_{0.4}\text{P}_{0.6}$  cap layer grown on the graded  $\text{InAs}_y\text{P}_{1-y}$  buffer layer at this magnification scale, indicating a threading dislocation density (TDD) in these  $\text{InAs}_{0.4}\text{P}_{0.6}$  layers on the order of or below  $\sim 10^7 \text{ cm}^{-2}$ . Figure 12(c) shows a representative XTEM image obtained from an  $\text{InAs}_{0.4}\text{P}_{0.6}$  single step structure on InP showing a high contrast at the film/substrate interface, and TDs can be observed in this  $\text{InAs}_{0.4}\text{P}_{0.6}$  layer. This reveals the presence of a high density of TDs for the direct-growth sample ( $> 10^7 \text{ cm}^{-2}$ ), as would be expected for single step growth of thick  $\text{InAs}_{0.4}\text{P}_{0.6}$  on InP due to the large lattice mismatch ( $\sim 1.3\%$ ). These TEM results demonstrate the high material quality of  $\text{InAs}_{0.4}\text{P}_{0.6}$  grown on InP using GBL and verify the high efficiency of InAsP graded buffers in migrating TDs during strain relaxation. Figure 13 shows the XTEM image of an  $\text{In}_{0.69}\text{Ga}_{0.31}\text{As}$  layer grown on an InP substrate using step-graded  $\text{InAs}_y\text{P}_{1-y}$  buffers, which is nominally lattice matched to the terminal relaxed InAsP layer lattice constant on InP. Again, no TDs are observed at this magnification. More accurate TD counting using plan-view TEM revealed average TDDs of  $\sim 2 \times 10^6 \text{ cm}^{-2}$  for  $\text{InAs}_{0.4}\text{P}_{0.6}$  films grown InP using GBL and  $\sim 1 \times 10^6 \text{ cm}^{-2}$  for the  $\text{In}_{0.69}\text{Ga}_{0.31}\text{As}$  overlayer, which are shown in Figs. 14(a) and 14(d), respectively, for growth on the graded  $\text{InAs}_y\text{P}_{1-y}/\text{InP}$  substrates. These values are used to determine dislocation velocities and dislocation spacing in these materials, discussed next. Note that the TDDs vary by more than a factor of  $10\times$  in the range of  $> 10^7 \text{ cm}^{-2}$  from area to area in the single step  $\text{InAs}_{0.4}\text{P}_{0.6}$  film on InP, as shown in Figs. 14(b) and 14(c), and these relatively large values of dislocation density are consistent with the x-ray peak broadening discussed earlier.

Properties such as dislocation velocities can be estimated using a model developed by Fitzgerald *et al.*<sup>27</sup> since the strain relaxation we have observed for these materials is glide limited. In this model, the relaxation rate of isotropic relaxed materials can be expressed as

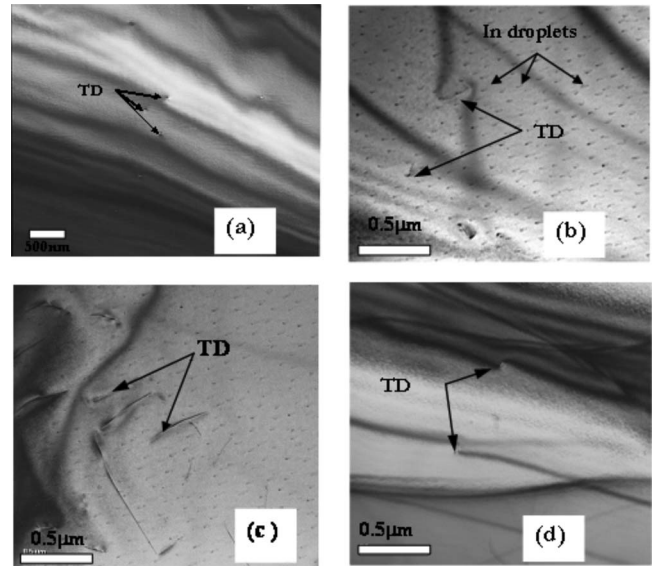


FIG. 14. Plan-view TEM micrographs of (a) an  $\text{InAs}_{0.4}\text{P}_{0.6}$  layer grown on a (001) InP using an  $\text{InAs}_y\text{P}_{1-y}$  step-graded buffer, [(b) and (c)] an  $\text{InAs}_{0.4}\text{P}_{0.6}$  layer directly grown on a (001) InP in two different areas of the film, and (d) an  $\text{In}_{0.69}\text{Ga}_{0.31}\text{As}$  overlayer grown on a  $2^\circ$  offcut (001) InP substrate. Black dots and black lines are due to indium droplets and bend contour, respectively.

$$\dot{\delta} = \frac{\rho_{\text{TDD}} v b}{4}, \quad (7)$$

where  $b$  is the Burgers vector for  $60^\circ$  dislocation and  $\rho_{\text{TDD}}$  is the TDD. The dislocation glide velocity  $v$  under an effective stress due to lattice mismatch (i.e., compressive stress) and growth temperature is given by<sup>42</sup>

$$v = B \left( \frac{Y \varepsilon_{\text{eff}}}{\tau_o} \right)^m \exp \left( - \frac{E_{\text{glide}}}{kT} \right), \quad (8)$$

where  $B$  and  $m$  ( $1 < m < 2$ ) are constants,  $\tau_o = 1 \text{ MPa}$ ,  $E_{\text{glide}}$  is the activation energy for dislocation glide,  $Y$  is the biaxial modulus, and  $\varepsilon_{\text{eff}}$  is the effective strain, assumed to be constant throughout the thickness of the graded layer. When the graded layer thickness is much larger than the critical layer thickness, the strain relieved from dislocation flow is approximately linear with thickness since the lattice mismatch through grading is almost linear with thickness; the TDD is given by<sup>27</sup>

$$\rho_{\text{TDD}} = \frac{2R_g R_{\text{gr}} \exp \left( \frac{E_{\text{glide}}}{kT} \right)}{b Y^m \varepsilon^m}, \quad (9)$$

where  $R_g$  is the growth rate and  $R_{\text{gr}}$  is the grading rate (mismatch per unit thickness). The growth parameters, such as the growth rate and the grading rate, can be varied to reduce the TDD to a lower limit. In applying this model to our case, some comments are necessary. First, the growth rate would not be changed by orders of magnitude if interested in device development. Second, the growth temperature cannot be increased significantly due to the higher vapor pressure of phosphorus as well as the higher composition of indium in the  $\text{In}_x\text{Ga}_{1-x}\text{As}$  overlayer and the temperature dependent surface sticking coefficients of both arsenic and phosphorus and

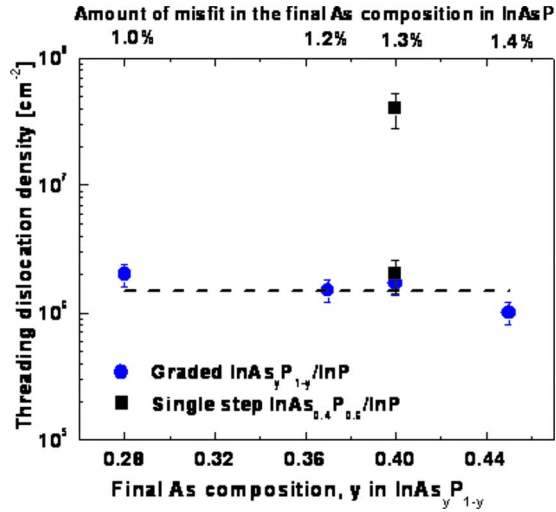


FIG. 15. (Color online) Threading dislocation densities as a function of the final arsenic composition obtained from plan-view TEM in InAs<sub>y</sub>P<sub>1-y</sub>/InP graded buffer layers. The field circle represents measured TDDs using plan-view TEM for graded InAs<sub>y</sub>P<sub>1-y</sub> layers, all of which were grown with the same grading coefficient and growth temperature, but with different ending arsenic compositions. A line was fitted through these data, and it was calculated using Eq. (9). The measured total misfit determined from XRD is also included in this figure, and note that the layers are more than 90% relaxed.

is fixed at 490 °C. Third, we note from earlier discussions in the paper that the measured (by plan-view TEM) TDDs are roughly constant for the InAs<sub>y</sub>P<sub>1-y</sub> buffers as a function of composition, approximately  $(1-2) \times 10^6 \text{ cm}^{-2}$ , indicative of well behaved metamorphic buffer behavior. With these comments now made, the measured TDD obtained for the various InAs<sub>y</sub>P<sub>1-y</sub>/InP GBLs as a function of arsenic composition ( $y$ ) in the final step of the grade is shown in Fig. 15. The circular data points with error bars are the measured TDD values. All structures used in this table were nominally grown with the same grading rate and growth temperature, the only difference being the final composition of the top-most layer. The line indicated in the figure is not an attempt to create a singular best fit to the data; in fact it is a calculation made using Eq. (9) with  $R_g=2.2 \text{ \AA/s}$ ,  $R_{gr}=3.23 \times 10^{-3}/0.4 \text{ \mu m}$ ,  $E_{\text{glide}}=1.75 \text{ eV}$ ,  $m=1.7$ ,  $B=1 \times 10^6 \text{ cm/s}$ ,  $Y=8.96 \times 10^{11} \text{ dyn/cm}^2$ , and  $\varepsilon_{\text{eff}}=1 \times 10^{-4}$ . Here, the biaxial modulus ( $Y$ ) was estimated using the values of InP and InAs with a linear interpolation, and the value of effective strain  $\varepsilon_{\text{eff}}$  is assumed to be constant throughout the thickness of the graded layer, and it should be less than the misfit value in each interface of step-graded InAsP buffer layer (this is reasonable to maintain the high strain relaxation and low density of TDs experimentally observed). A constant moderate value of effective strain during epitaxy is needed; otherwise, any decrease in effective strain created by impediments to dislocation glide will increase the TDD drastically. With these assumptions, it still must be noted that both  $B$  and  $E_{\text{glide}}$  are unknown variables; thus different combinations of values can be used to fit the data such that an accurate determination of  $E_{\text{glide}}$  is not possible and the line shown in the figure is one of multiple fits. However, we know that  $E_{\text{glide}}$  for InAs<sub>y</sub>P<sub>1-y</sub> must be bounded by its values for InP and InAs, and we also know from Eq. (9) that  $\rho_{\text{TDD}}$  only weakly depends on  $B$ .

Hence relative larger changes in  $B$  will only generate small changes in  $E_{\text{glide}}$ , and thus we can estimate the glide activation energy from Fig. 15 as described above. Regardless of the accuracy of  $E_{\text{glide}}$ , the close fit between the glide-limited dislocation dynamics model and the experimental data, which is the purpose of this discussion, clearly suggests the absence of impediments to dislocation glide in these graded buffer layers and supports the assertion that these buffers indeed relax in a glide-limited process.

Finally, to assess the possible presence of dislocation-dislocation interactions on strain relaxation, we have considered a relationship between the dislocation length and the dislocation density. Such a relationship is necessary for an accurate determination of average dislocation length because of the limited field of view of the plan-view TEM images of the upper final arsenic-composition layer in InAs<sub>y</sub>P<sub>1-y</sub> GBL. Here we assume that the average dislocation length is much less than the diameter of the wafer and that there are two orthogonal misfit dislocation arrays present, each with the same average misfit dislocation length,  $L$ . In this case, misfit dislocations should be arranged periodically in the interface to accommodate lattice mismatch, and the misfit dislocation spacing  $L$  can be calculated using the equation<sup>43</sup>

$$L = \left| \frac{1 + \varepsilon}{\varepsilon} \right| b_{\text{misfit}}. \quad (10)$$

Using the relaxed layer lattice constant determined from Eq. (1) and the misfit strain from Eq. (2) for the single step InAs<sub>0.4</sub>P<sub>0.6</sub> layer on InP, the calculated misfit dislocation spacing is about 163 Å. This spacing is larger for the InAs<sub>0.4</sub>P<sub>0.6</sub> layer grown on InP using step-graded InAs<sub>y</sub>P<sub>1-y</sub> compared to the single step structure since the misfit dislocation density is distributed among four interfaces for the graded InAs<sub>y</sub>P<sub>1-y</sub> buffer. It is interesting to note that the misfit dislocation spacing is on the order of device geometries for next generation nanoelectronics, suggesting the possible development of dislocation-free devices that can make use of lattice mismatched III-V materials that are grown on well-controlled metamorphic substrates based on anion-graded III-V materials.

#### D. Surface morphology

It is important to characterize the surface morphology (roughness and other possible features) for metamorphic structures due to the expected crosshatch resulting from ideal strain relaxation with minimum concentrations of TDs, as this is an important figure of merit. AFM images and line profiles in two orthogonal  $\langle 110 \rangle$  directions of the relaxed InAs<sub>0.4</sub>P<sub>0.6</sub> surface grown on InAsP buffers on both (100) and offcut InP substrates are shown in Figs. 16 and 17, respectively. From these figures, the anticipated two-dimensional crosshatch pattern is well developed and extremely uniform, as expected for an ideal graded buffer. The peak-to-valley height from line profiles in the two  $\langle 110 \rangle$  orthogonal dislocation directions is also included in these figures. This bidirectionally uniform crosshatch pattern from the surfaces of graded InAs<sub>y</sub>P<sub>1-y</sub> buffers on (100) or 2°

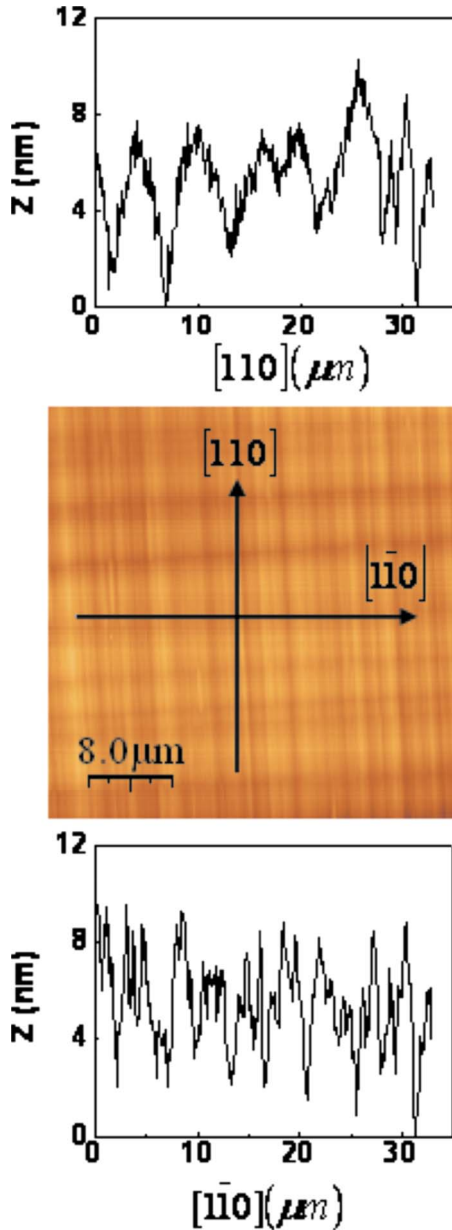


FIG. 16. (Color online) AFM image and line profile in two  $\langle 110 \rangle$  directions of an  $\text{InAs}_{0.4}\text{P}_{0.6}$  layer grown on a (001) InP substrate using an  $\text{InAs}_y\text{P}_{1-y}$  step-graded buffer.

offcut InP substrate is an indication of symmetric relaxation, in complete agreement with the XRD results and analysis presented above. The surface *rms* roughness of the  $\text{InAs}_{0.4}\text{P}_{0.6}$  layers grown on both (100) and  $2^\circ$  offcut (100) InP substrates using a graded  $\text{InAs}_y\text{P}_{1-y}$  buffer is  $\sim 3.2$  and  $\sim 3.4$  nm, respectively, measured over an area of  $40 \times 40 \mu\text{m}^2$ . The *rms* roughness of the  $\text{InAs}_y\text{P}_{1-y}$  graded buffer is almost identical on both types of InP substrates and is significantly lower than layers grown on cation-graded buffers over the same misfit range on the same initial substrates,<sup>1</sup> which is attributed to advantages of grading on the group-V anion sublattice, as discussed earlier in this paper.

#### IV. CONCLUSIONS

The strain relaxation behavior and defect properties of MBE-grown, compositionally graded  $\text{InAs}_y\text{P}_{1-y}$  buffers

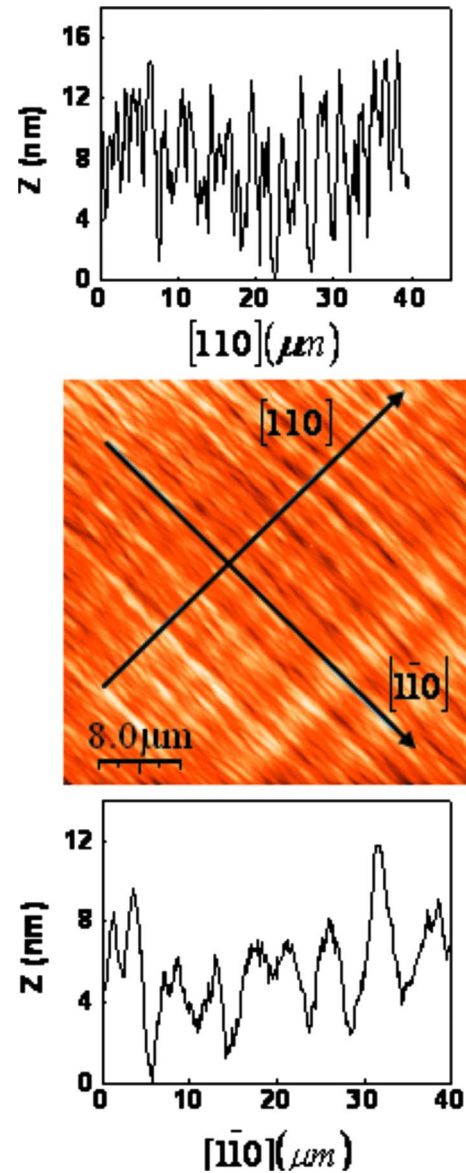


FIG. 17. (Color online) AFM image and line profile in two  $\langle 110 \rangle$  directions of an  $\text{InAs}_{0.4}\text{P}_{0.6}$  layer grown on a  $2^\circ$  offcut (001) InP substrate using an  $\text{InAs}_y\text{P}_{1-y}$  step-graded buffer.

grown on (001) and offcut (001) InP substrates, with the lattice misfit ranging from 1% to 1.4%, and of their utility to provide a virtual substrate for subsequent lattice matched  $\text{In}_{0.69}\text{Ga}_{0.31}\text{As}$  overlayers have been investigated. For both on- and off-axis substrates, the strain relaxation was found to be both symmetric and glide limited. The nearly ideal compressive strain relaxation behavior observed was shown to correlate with low TD values that do not vary with misfit over this range. We attribute this behavior in part to the efficient use of residual dislocations by the higher misfit layers, with dislocation glide, and not dislocation nucleation kinetics, being the limiting factor for strain relaxation in the In-AsP system up to at least the misfit magnitude with respect to InP that was explored here. As a result, MBE-grown anion-graded  $\text{InAs}_y\text{P}_{1-y}$  step-graded buffers are a promising virtual substrate technology for extending the performance and application of InP-based infrared and high speed device appli-

cations since they provide access to various combinations of band gaps and band offset energies while maintaining high material quality.

## ACKNOWLEDGMENTS

The authors would like to thank Hendrick Colijn (Ohio State University) for FIB sample preparation, Kevin Matney (Bede Scientific) for x-ray topography, and C. Tivarus (Ohio State University) for AFM measurements. This work is supported in part by National Science Foundation (Focused Research Group) under Grant No. DMR-0313468, by the U.S. Air Force Office of Scientific Research (K. Reinhardt), and by the U.S. Army Research Office (J. Prater).

- <sup>1</sup>M. K. Hudait, Y. Lin, M. N. Palmisiano, C. A. Tivarus, J. P. Pelz, and S. A. Ringel, *J. Appl. Phys.* **95**, 3952 (2004).
- <sup>2</sup>M. K. Hudait, Y. Lin, M. N. Palmisiano, and S. A. Ringel, *IEEE Electron Device Lett.* **24**, 538 (2003).
- <sup>3</sup>M. W. Wanlass, J. J. Carapella, A. Duda, K. Emery, L. Gedvilas, T. Moriarty, S. Ward, J. D. Webb, and X. Wu, Fourth NREL Conference on TPV Generation of Electricity, AIP, 1999, Vol. 460, p. 132.
- <sup>4</sup>N. S. Fatemi, D. M. Wilt, R. W. Hoffman, Jr., M. A. Stan, V. G. Weizer, P. P. Jenkins, O. S. Khan, C. S. Murray, D. Scheiman, and D. Brinker, Fourth NREL Conference on TPV Generation of Electricity, AIP, 1999, Vol. 460, p. 121.
- <sup>5</sup>B. Wernsman, T. Bird, M. Sheldon, S. D. Link, and R. Wehrer, *J. Vac. Sci. Technol. B* **24**, 1626 (2006).
- <sup>6</sup>S. L. Murray, F. D. Newman, D. M. Wilt, M. W. Wanlass, P. Ahrenkiel, R. Messham, and R. R. Siegiej, *Semicond. Sci. Technol.* **18**, S202 (2003).
- <sup>7</sup>A. Krier, D. Chubb, S. E. Krier, M. Hopkinson, and G. Hill, *IEE Proc.: Optoelectron.* **145**, 292 (1998); R. U. Martinelli, T. J. Zamerowski, and P. A. Longeway, *Appl. Phys. Lett.* **54**, 277 (1989).
- <sup>8</sup>M. D'Hondt, I. Moreman, P. Van Daele, and P. Demeester, *IEE Proc.: Optoelectron.* **144**, 277 (1997).
- <sup>9</sup>K. R. Linga, G. H. Olen, V. S. Ban, A. M. Joshi, and W. F. Kosonocky, *J. Lightwave Technol.* **10**, 1050 (1992).
- <sup>10</sup>M. D. Lange, A. Cavus, C. Monier, R. S. Sandhu, T. R. Block, V. F. Gambin, D. J. Sawdai, and A. L. Gutierrez-Aitken, *J. Vac. Sci. Technol. B* **22**, 1570 (2004).
- <sup>11</sup>R. S. Goldman, K. L. Kavanagh, H. H. Wieder, S. N. Ehrlich, and R. M. Feenstra, *J. Appl. Phys.* **83**, 5137 (1998) and references therein.
- <sup>12</sup>R. S. Goldman, H. H. Wieder, and K. L. Kavanagh, *Appl. Phys. Lett.* **67**, 344 (1995).
- <sup>13</sup>R. S. Goldman, H. H. Wieder, K. L. Kavanagh, K. Rammohan, and D. H. Rich, *Appl. Phys. Lett.* **65**, 1424 (1994).
- <sup>14</sup>B. R. Bennett and J. A. DelAlamo, *J. Electron. Mater.* **20**, 1075 (1991).
- <sup>15</sup>V. Krishnamoorthy, Y. W. Lin, L. Calhoun, H. L. Liu, and R. M. Park, *Appl. Phys. Lett.* **61**, 2680 (1992).
- <sup>16</sup>J. A. Olsen, E. L. Hu, S. R. Lee, I. J. Fritz, J. Howard, B. E. Hammons, and J. Y. Tsao, *J. Appl. Phys.* **79**, 3578 (1996).
- <sup>17</sup>J.-I. Chyi, J.-L. Shieh, J.-W. Pan, and R.-M. Lin, *J. Appl. Phys.* **79**, 8367 (1996).
- <sup>18</sup>J.-M. Chauveau, Y. Androussi, A. Lefebvre, J. Di Persio, and Y. Cordier, *J. Appl. Phys.* **93**, 4219 (2003).
- <sup>19</sup>M. J. Matragrano, D. G. Ast, J. R. Shealy, and V. Krishnamoorthy, *J. Appl. Phys.* **79**, 8371 (1996).
- <sup>20</sup>K. L. Kavanagh, J. C. P. Chang, J. Chen, J. M. Fernandez, and H. H. Wieder, *J. Vac. Sci. Technol. B* **10**, 1820 (1992).
- <sup>21</sup>A. Y. Kim, W. S. McCullough, and E. A. Fitzgerald, *J. Vac. Sci. Technol. B* **17**, 1485 (1999).
- <sup>22</sup>M. K. Hudait, Y. Lin, D. M. Wilt, J. S. Speck, C. A. Tivarus, E. R. Heller, J. P. Pelz, and S. A. Ringel, *Appl. Phys. Lett.* **82**, 3212 (2003).
- <sup>23</sup>M. K. Hudait, Y. Lin, P. M. Sinha, J. R. Lindemuth, and S. A. Ringel, *J. Appl. Phys.* **100**, 063705 (2006).
- <sup>24</sup>Y. Lin, J. A. Carlin, A. R. Arehart, A. M. Carlin, and S. A. Ringel, *Appl. Phys. Lett.* **90**, 012115 (2007).
- <sup>25</sup>Y. Lin, A. R. Arehart, A. M. Carlin, and S. A. Ringel, *Appl. Phys. Lett.* **93**, 062109 (2008).
- <sup>26</sup>M. W. Wanlass, J. S. Ward, K. A. Emery, M. M. Al-Jassim, K. M. Jones, and T. J. Coutts, *Sol. Energy Mater. Sol. Cells* **41–42**, 405 (1996).
- <sup>27</sup>E. A. Fitzgerald, A. Y. Kim, M. T. Currie, T. A. Langdo, G. Taraschi, and M. T. Bulsara, *Mater. Sci. Eng., B* **67**, 53 (1999).
- <sup>28</sup>C. Priester and G. Grenet, *Phys. Rev. B* **61**, 16029 (2000).
- <sup>29</sup>F. Romanato, E. Napolitani, A. Carnera, A. V. Drigo, L. Lazzarini, G. Salvati, C. Ferrari, A. Bosacchi, and S. Franchi, *J. Appl. Phys.* **86**, 4748 (1999).
- <sup>30</sup>S. I. Molina, F. J. Pacheco, D. Araujo, R. Garcia, A. Sacedon, E. Calleja, Z. Yang, and P. Kidd, *Appl. Phys. Lett.* **65**, 2460 (1994).
- <sup>31</sup>J. C. P. Chang, J. Chen, J. M. Fernandez, H. H. Wieder, and K. L. Kavanagh, *Appl. Phys. Lett.* **60**, 1129 (1992).
- <sup>32</sup>M. S. Goorsky, J. W. Eldredge, S. M. Lord, and J. S. Harris, *J. Vac. Sci. Technol. B* **12**, 1034 (1994).
- <sup>33</sup>S. P. Ahrenkiel, M. W. Wanlass, J. J. Carapella, L. M. Gedvilas, B. M. Keyes, R. K. Ahrenkiel, and H. R. Moutinho, *J. Electron. Mater.* **33**, 185 (2004).
- <sup>34</sup>M. W. Dashiell, H. Ehsani, P. C. Sander, F. D. Newman, C. A. Wang, Z. A. Shellenbarger, D. Donetski, N. Gu, and S. Anikeev, *Sol. Energy Mater. Sol. Cells* **92**, 1003 (2008).
- <sup>35</sup>T. Okada, R. V. Kruzelecky, G. C. Weatherly, D. A. Thompson, and B. J. Robinson, *Appl. Phys. Lett.* **63**, 3194 (1993).
- <sup>36</sup>T. Marschner, M. R. Leys, H. Vonk, and J. H. Wolter, *Physica E (Amsterdam)* **2**, 873 (1998).
- <sup>37</sup>S.-W. Ryu, H.-D. Kim, S.-K. Park, W. G. Jeong, and B.-D. Choe, *Jpn. J. Appl. Phys., Part 2* **36**, L79 (1997).
- <sup>38</sup>M. Dynna, T. Okada, and G. C. Weatherly, *Acta Metall. Mater.* **42**, 1661 (1994).
- <sup>39</sup>V. Swaminathan and A. T. Macrander, *Materials Aspects of GaAs and InP Based Structures* (Prentice-Hall, Englewood Cliffs, NJ, 1991).
- <sup>40</sup>H. Ehsani, I. Bhat, R. J. Gutmann, G. Charache, and M. Freeman, *J. Appl. Phys.* **86**, 835 (1999).
- <sup>41</sup>F. K. LeGoues, B. S. Meyerson, J. F. Morar, and P. D. Kirchner, *J. Appl. Phys.* **71**, 4230 (1992); F. K. LeGoues, P. M. Mooney, and J. O. Chu, *Appl. Phys. (Berlin)* **62**, 140 (1993).
- <sup>42</sup>E. A. Fitzgerald, Y.-H. Xie, D. Monroe, P. J. Silvennan, J.-M. Kuo, A. R. Kortan, F. A. Thiel, B. E. Weir, and L. C. Feldman, *J. Vac. Sci. Technol. B* **10**, 1807 (1992).
- <sup>43</sup>Y. X. Chen, C. Y. Cui, Z. Q. Liu, L. L. He, J. T. Guo, and D. X. Li, *J. Mater. Res.* **15**, 1261 (2000).